

RSC Advances

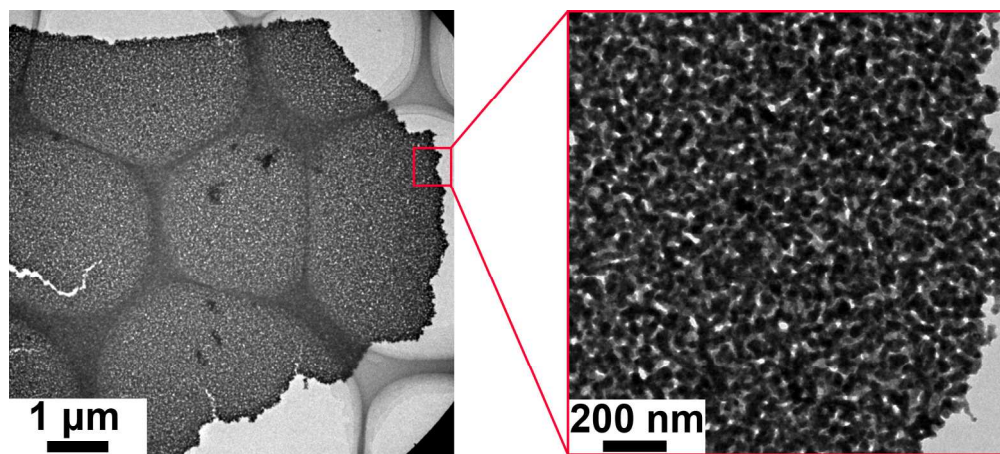


This is an *Accepted Manuscript*, which has been through the Royal Society of Chemistry peer review process and has been accepted for publication.

Accepted Manuscripts are published online shortly after acceptance, before technical editing, formatting and proof reading. Using this free service, authors can make their results available to the community, in citable form, before we publish the edited article. This *Accepted Manuscript* will be replaced by the edited, formatted and paginated article as soon as this is available.

You can find more information about *Accepted Manuscripts* in the [Information for Authors](#).

Please note that technical editing may introduce minor changes to the text and/or graphics, which may alter content. The journal's standard [Terms & Conditions](#) and the [Ethical guidelines](#) still apply. In no event shall the Royal Society of Chemistry be held responsible for any errors or omissions in this *Accepted Manuscript* or any consequences arising from the use of any information it contains.



Cu-Ag bimetallic porous nanomembranes, prepared by chemical dealloying and ultrasonic vibration, exhibit an thickness of about 5~50 nm, pore diameters of ~10-20 nm and ligament feature sizes of ~30-50 nm.
180x80mm (300 x 300 DPI)



Journal Name

ARTICLE

Novel Cu-Ag Bimetallic Porous Nanomembrane Prepared From A Multi-component Metallic Glass†

Received 00th January 20xx,
Accepted 00th January 20xx

Xue Liu,^a Na Chen,^a Jia-Lun Gu,^a Jing Du^b and Ke-Fu Yao*^a

DOI: 10.1039/x0xx00000x

www.rsc.org/

Porous nanomembranes (PNMs) have wide applications in templates, filtration, transport and separation, water treatment, drug delivery and sensing, but the preparation of metallic PNMs has been scarcely reported due to the technical difficulty and the easy oxidization during the preparation and preservation processes. In present work, ultrathin Cu-Ag bimetallic PNMs with an thickness of about 5~50 nm, an area larger than 20 square micron, pore diameters of ~10-20 nm and ligament feature sizes of ~30-50 nm have been prepared from a $Zr_{48}Cu_{36}Ag_8Al_8$ metallic glass by chemical dealloying assisted with ultrasonic vibration. The structural evolution and formation mechanism of the Cu-Ag bimetallic PNMs were also investigated. The effects of dealloying parameters on the dealloyed samples' morphology were systematically investigated. The prepared Cu-Ag bimetallic PNMs exhibit good antibacterial activity against *E. coli* over a wide concentration range. The present result provides an easy and inexpensive method for preparing Cu-Ag PNMs.

Introduction

Nanostructured materials have attracted great attentions due to their excellent catalytic, electrical, magnetic, optical and antibacterial properties, which are determined by their morphology and surface chemistry.¹⁻⁴ Many techniques have been developed to prepare nanostructured materials, such as dealloying,⁵ mechanical exfoliation,⁶ chemical vapor deposition (CVD)⁷ and physical vapor deposition (PVD),⁸ sol-gel method,⁹ electric-arc and arc-discharge methods,¹¹⁻¹³ aqueous solution method,¹⁴ selective etching,^{15, 16} vapor-liquid-solid (VLS) method,¹⁷ nanoimprinting^{18, 19} and so on. By these techniques, nanostructures with different morphologies, such as nanoparticles, nanotubes, nanowires, nanosheets, nanofibers and nanoribbons have been successively prepared.

Nanomembranes possess wide applications in templates,²⁰ filtration,²² transport and separation,^{23, 24} water treatment,²⁵ drug delivery,²⁶ and sensing.²⁷ However, the preparation of metallic porous nanomembrane (PNM) has been scarcely reported due to the technical difficulty and the easy oxidization during the preparation and preservation processes.²⁸ Then it's meaningful to develop new techniques and new methods for their synthesis. Copper and silver nanostructures are widely used in electronic devices, sensors, catalysts and

antibacterial materials.²⁹⁻³¹ In particular, the bimetallic Cu-Ag nanostructures exhibit superior antibacterial performance.^{29, 30} However, there is still no effective method for the preparation of Cu-Ag bimetallic PNMs. The search for a facile and low-cost approach to synthesis of Cu-Ag bimetallic PNMs is thus imperative from a viewpoint of practical applications.

Development in various metal-based alloys, metallic glasses (MGs) possess uniform and isotropic structures down to sub-nanometer scale.² This unique structural homogeneity enables them to be very suitable for synthesizing nanostructures by the dealloying method.^{2, 32} In present work, we report a facile and low-cost method, namely a combination of dealloying and ultrasonic vibration of a $Zr_{48}Cu_{36}Ag_8Al_8$ MG ribbon, for preparing Cu-Ag bimetallic PNMs. In addition, the antibacterial property of the Cu-Ag PNMs was investigated.

Results and discussion

Synthesis and characterization of Cu-Ag bimetallic PNMs

Synthesis of Cu-Ag bimetallic PNMs. When the dealloying process began, gas bubbles started to emerge on the surfaces of the sample, and then the colour of the samples gradually turned into golden yellow. After dealloyed in 0.05 M hydrofluoric acid for 24 h, there are no more gas bubbles produced on the sample surface and the colour of the sample didn't change any more, indicating that the dealloying process is finished. The completely dealloyed sample is quite brittle, but can be carefully handled with tweezers. The optical photograph of the completely dealloyed sample with a dimension of ~30 mm×8 mm is shown in Fig. S1 in ESI †, where the sample appears golden yellow and some delaminating can be clearly seen.

^a Key Lab of Advanced Materials Processing Technology of Ministry of Education, School of Materials Science and Engineering, Tsinghua University, Beijing 100084, China. E-mail: kfyao@tsinghua.edu.cn; Tel:+86-10-62772292; Fax: +86-10-62771160.

^b Institute of Biomechanics and Medical Engineering, School of Aerospace, Tsinghua University, Beijing 100084, China.

† Electronic Supplementary Information (ESI) available: [Optical image of the dealloyed sample, SEM images of the dealloyed sample, EDS result of the dealloyed sample and TEM bright field image of the Cu-Ag bimetallic PNM]. See DOI: 10.1039/x0xx00000x

Table 1. The calculated grain sizes of the dealloyed sample.

2θ (degree)	Crystal Indices	Full Width of Half Maximum (degree)	Calculated grain size (nm)	Average Grain Size (nm)
38.20	(111) _{Ag}	0.48	17.3	16.1
64.57	(220) _{Ag}	0.62	14.9	
43.37	(111) _{Cu}	0.17	49.1	39.3
50.50	(200) _{Cu}	0.4	21.9	
74.19	(220) _{Cu}	0.21	46.8	

X-ray diffraction (XRD) characterization. Fig. 1a shows the XRD spectra of the as-prepared $Zr_{48}Cu_{36}Ag_8Al_8$ ³³ MG ribbon and the dealloyed sample. The absence of any sharp diffraction peak in the XRD spectrum of the MG ribbon indicates its glass structure. While in the XRD spectrum of the dealloyed sample, peaks corresponding to Cu and Ag emerge, revealing that the dealloyed sample consists of face centered cubic (FCC) Cu and Ag phases. It is noticed that the diffraction peaks corresponding to Cu and Ag are somehow broad, indicating the existence of size-limited phases. After deconvoluting the beam size effect, the grain sizes could be calculated based on the Scherrer Formula, and the results are listed in Table 1. It can be seen that the average grain size of the Ag is 16.1 nm, and that of the Cu is 39.3 nm. Thus, the dealloyed sample possesses very fine grains.

Scanning electron microscope (SEM) characterization. Fig. 1b shows the SEM image of the dealloyed sample, where some cracks are found, and typical feature size of the dealloyed structure is ~dozens of microns. After folding the dealloyed sample is easily broken into pieces, and sheet structures with thickness varies from ~100 nm to ~1 μm are observed, as shown in Fig. S2 in ESI †. The formation of the sheet structures indicates the existence of delaminating in the dealloyed sample. Since there is corrosion stress generated in the dealloying process, the delaminating is probably related to the stress.

The enlarged SEM images of the dealloyed sample are shown in Fig. 1c and d, where uniform nanoporous structure are observed. The size of the pores was measured to be ~10-20 nm and that of the ligaments was measured to be ~30-50 nm. With the help of energy dispersive spectrometer (EDS) in SEM, the composition of the dealloyed sample was confirmed to be $Cu_{84}Ag_{13}O_3$ (seeing Fig. S3 in ESI †). Since Cu_2O is quite easy to be formed in copper nanostructures,³⁴ the very low content of oxygen should be caused by the diffusely distributed silver. The XRD and the SEM results indicate that the dealloyed sample is of Cu-Ag nanoporous structures.

Transmission electron microscopy (TEM) characterization. After the ultrasound treatment, the Cu-Ag nanoporous sheet structure turned to be PNMs with area larger than 20 square microns. The bright field TEM image of a typical PNM is shown in Fig. 2a. The selected area electron diffraction (SAED) pattern in the inset of Fig. 2a shows diffused halo rings around the central bright spot, which indicates the very fine grains in the

PNM and is consistent with the XRD results. In Fig. 2b and c, uniform pores with diameters of ~10-20 nm and the ligaments with diameter of ~30-50 nm were observed, which are consistent with the SEM results.

The sub-nanosize structure of the PNM has been inspected by high resolution transmission electron microscopy (HRTEM), and a typical image is presented in Fig. 2d. No detectable oxide layers can be seen and clear lattices are observed. After measurement, the interplanar distances of 2.3-2.5 Å and 2.1 Å were indexed, which correspond to the interplanar spacings of {111} planes of Ag and Cu, respectively. The HRTEM results are consistent with the XRD result and further prove that the PNM is made of Cu and Ag phases. The obtained clear HRTEM image suggests that the thickness of the thin area of the PNM is less than 10 nm.¹⁵ According to the TEM bright field images showing in Fig. 2, the whole thickness of the PNM is roughly estimated as 5~50 nm. Thus, by simple chemical roughly assisted with ultrasonic vibration, Cu-Ag bimetallic PNMs were successfully prepared. Since the Cu-Ag bimetallic PNMs are quite stable even after suffered from the ultrasonic vibration, the present work provided an easy and cheap method for preparing stable Cu-Ag PNMs.

During the TEM investigation, some Cu-Ag PNMs with much larger thickness have also been noticed, as shown in Fig. S4 in ESI †. At the edge of the thick PNM, ultrathin PNMs can be clearly seen. Associating it with the sheet structure observed in Fig. 1b, it can be found that the PNMs are evaluated from the sheet structures. During the ultrasound treatment, the sheet structure further delaminates and then PNMs are exfoliated. Therefore, thick PNM with ultrathin PNMs on the edges are formed on the area where delaminating is not complete.

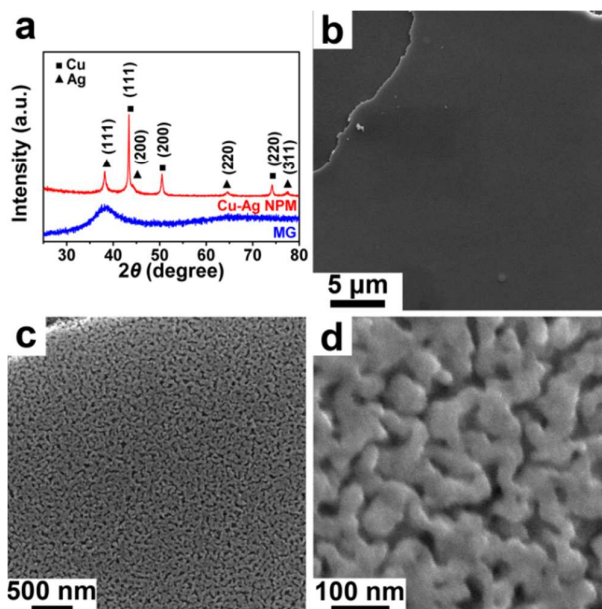


Fig. 1 (a) XRD spectra of the as-prepared MG sample and the dealloyed Cu-Ag NPM. (b)-(d) SEM images of the dealloyed sample with different magnifications.

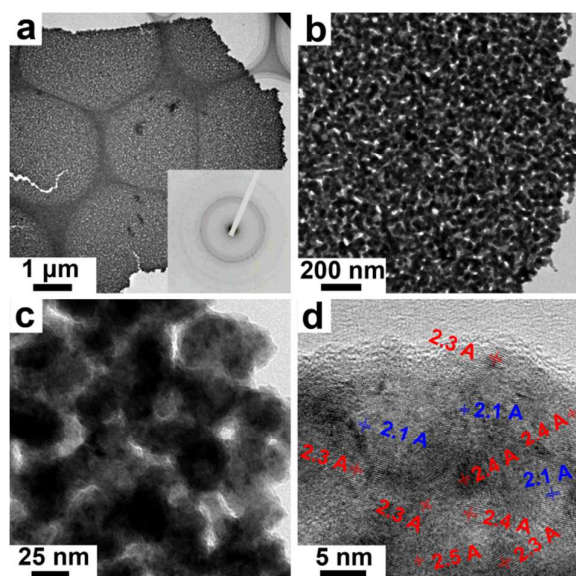


Fig. 2 Bright field TEM images (a-c) and HRTEM image (d) of the Cu-Ag bimetallic PNM. The inset in (a) is the SAED pattern of the PNM.

Effects of dealloying parameters on the morphology of the dealloyed samples.

Effects of dealloying time. Since the dealloying time has significantly influence on the sample's morphology,⁵ the effects of the dealloying time were investigated. After dealloyed by 0.05 M hydrofluoric acid for 1 h, 3 h, 6 h and 12 h, the morphologies of the dealloyed samples were investigated, respectively. After dealloyed for 1 h, uniform nanopores with relatively low density are formed on the sample surface, as shown in Fig. 3a. The nanopores possess diameters of ~5-10 nm, and are separated from each other. With extending the dealloying time to 3 h, the diameters of the nanopores increase to ~10-15 nm, as shown in Fig. 3b. Compared with the nanopores obtained by dealloying for 1 h, the density of the nanopores significantly increases, and several nanopores start to connect with each other. With further extending the dealloying time, the density of the nanopores keeps increasing. Thus, more and more nanopores start to connect to each other. When the dealloying time is longer than 6 h, almost all the nanopores are interconnected with each other, and the pore size expands to ~10-20 nm. Accordingly, extending the dealloying time increases the diameter and density of the nanopores. Meanwhile, the morphology of the nanopores transforms from the separated nanopores to the interconnected ones. The expanding and interconnecting of the nanopores are caused by the continual dissolution of Zr/Al atoms and the diffusion of Cu/Ag atoms, which is a common phenomenon in dealloying.³⁵

The inserts in Fig. 3 show the low-magnification SEM images of the corresponding dealloyed samples. All the samples are incompletely dealloyed, and silvery MG can be seen from the fracture faces. With the help of EDS in SEM, the nanoporous structures are all confirmed to be made of Cu and Ag. Then the samples present a sandwich-like structure of

nanoporous Cu-Ag/MG/nanoporous Cu-Ag. Sheet structures caused by delaminating are noticed in all of the dealloyed samples. Similar to that in the sample dealloyed for 12 h, the thickness of sheet structures varies from ~100 nm to 1 μm in each dealloyed sample. No obvious interrelation between the dealloying time and the thickness is found. This phenomenon suggests that Cu-Ag sheet structures with thickness of ~100 nm-1 μm, rather than Cu-Ag PNMs with thickness below 100 nm, are formed during the dealloying process. The PNMs are suggested to be formed during the ultrasonic vibration process.

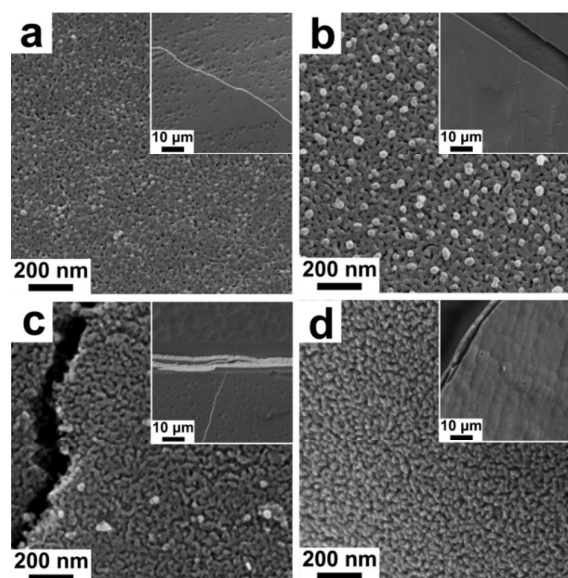


Fig. 3 SEM images of the $Zr_{48}Cu_{36}Ag_8Al_8$ MG ribbon samples dealloyed by 0.05 M hydrofluoric acid for different time. (a) 1 h, (b) 3 h, (c) 6 h and (d) 12 h. The inserts are the corresponding low-magnification images.

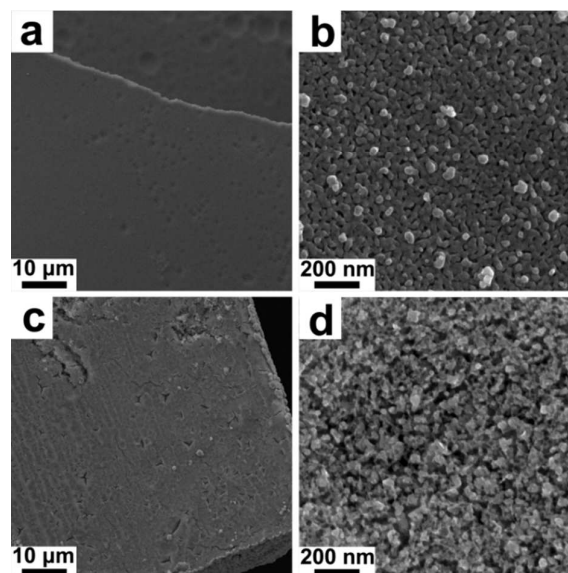


Fig. 4 SEM images of the sample dealloyed by hydrofluoric acid with different concentrations for 24 h. (a) 0.01 M hydrofluoric acid. (b) is the enlarge image of (a). (c) 0.2 M hydrofluoric acid. (d) is the enlarge image of (c).

Effects of the dealloying solution's concentration. It has been reported that the concentration of the dealloying solution has significant influence on the morphology of the dealloyed sample.³⁴ Fig. 4a and 4b show the SEM images of the sample dealloyed in 0.01 M hydrofluoric acid for 24 h. The sample is also incompletely dealloyed as the one dealloyed in 0.05 M (Fig. 3). Sheet structures with variable thickness of ~ 100 nm–1 μ m are observed on the sample surface. Nanoporous structure with diameters of ~ 10 –15 nm can be seen in Fig 4b. Several nanopores contact with each other to form the interconnected nanopores, which is similar to the morphology of the sample dealloyed in 0.05 M for 3 h. The above results indicate that diluting the dealloying solution reduces the size and the density of the nanopores, similar to reducing the dealloying time. Smaller sized nanopores thus tend to separate from each other.

The SEM image of the sample dealloyed in 0.2 M hydrofluoric acid for 24 h is shown in Fig. 4c, where the sample is completely dealloyed and no sheet structures caused by delaminating can be found. Fig. 4d shows the enlarged image of Fig. 4c, where developed nanoporous structure with diameters of ~ 20 –50 nm and some nanocracks can be seen. It has been reported that the dealloying rate can be promoted by increasing the concentration of the dealloying solution.³⁴ Increasing the dealloying rate leads to the change of the interfacial kinetics, and then makes the nanopore expand.³⁴ When the sizes of these nanopores increase to a certain value, nanocracks form with the merging of the nanopores. Then the stress can be released through the nanocracks, leading to the suppression of the delaminating. Therefore, with increasing the concentration of the dealloying solution, the sizes of the nanopores become larger, and the delaminating of the nanoporous structure is suppressed.

Effects of the MG's stress state. It is well known that there exists residual stress in the MG ribbons due to the rapid solidification process. In addition, the stress could be also introduced during the dealloying process. Thus, the morphology of the dealloyed sample may be related to the stress effect. To uncover the effect of the MG's stress state on the dealloyed sample's morphology, a bulk $Zr_{48}Cu_{36}Ag_8Al_8$ MG sample was annealed at T_g (417 K) for 30 min to eliminate the residual stress, and then dealloyed in 0.05 M hydrofluoric acid for 24 h. After dealloying, similar Cu–Ag nanoporous structure is obtained, as shown in Fig. 5a. Fig. 5b presents the low-magnification SEM image of Fig. 5a, where Cu–Ag sheet structure can be observed on the surface of the dealloyed sample. However, the thicknesses of the sheet structures are measured to be ~ 5 –10 μ m. Since the dealloying condition is the same as that of the MG ribbon without annealing, the significant increase of the sheet structure's thickness is supposed to be closely related to the change of the stress state.

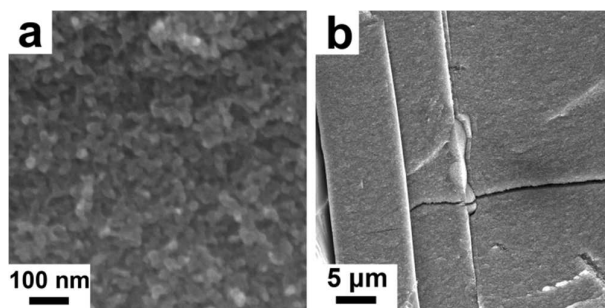


Fig. 5 (a) The high-magnification and (b) low-magnification SEM images of the annealed MG sample dealloyed in 0.05 M hydrofluoric acid for 24 h.

It is suggested that there exists a critical stress value for the delaminating and subsequent formation of the sheet structure. Due to the absence of channels such as grain boundaries for releasing the stress in the MGs, the corrosion stress can be accumulated during the dealloying process. In the as-prepared $Zr_{48}Cu_{36}Ag_8Al_8$ MG ribbon sample, the critical stress value could be rapidly achieved under the synergy effects of the residual stress and corrosion stress. This results in the formation of the sheet structures associated with the activation of the delaminating. While in the annealed bulk sample, the absence of residual stress delays the access to the critical stress value, attributed to the formation of sheet structures with a much larger thickness.

Formation mechanism of the Cu–Ag bimetallic PNMs

The formation mechanism of the Cu–Ag bimetallic PNMs can be proposed based on the above results. Fig. 6 illustrates the structural evolution of the Cu–Ag bimetallic PNMs. During the chemical dealloying, both Zr and Al atoms are etched out from both sides of the $Zr_{48}Cu_{36}Ag_8Al_8$ ribbon whereas Cu and Ag atoms remain to form the nanoporous structure with very fine pore size. Similar to the conventional dealloying,³⁵ the pore size and the density of the nanopores increase with prolonging the dealloying time. Consequently, the neighbouring nanopores start to merge together to form the interconnected nanopores, as displayed in Fig. 6a. Since MGs have uniform structures down to nanoscale,^{2,3} the stress produced by rapid solidification and dealloying can't be released through defects such as grain boundaries. After the dealloying depth reaches a certain value, the critical stress value for the activation of the delaminating is achieved due to the synergy effects of the residual stress and corrosion stress. Then the delaminating occurs on the surface of the nanoporous structure (Fig. 6b). After the dealloying is completely finished, the delaminating dominates the structural development, and can be directly seen on the sample, as shown in Fig. S1 in ESI †. After the ultrasound treatment, the sheet structures are peeled off from the matrix (Fig. 6c). Then the further delaminating is activated under the action of the supersonic vibration, and the PNMs with ultrathin thickness are formed, as displayed in Fig. 6d and 6e. However, when increasing the solution concentration, the dealloying rate gets faster, and nanocracks form. Then the stress will be released through the nanocracks, leading to the absence of the sheet structures and PNMs, as shown in Fig. 5c and 5d.

Since the composition of the MGs can be designed, by selecting proper MGs and dealloying conditions, various multicomponent PNMs could be synthesized through the simple chemical dealloying assisted with ultrasonic vibration.

Antibacterial activities of the Cu-Ag bimetallic PNMs

Fig. 7a shows the representative growth profiles in the presence of Cu-Ag bimetallic PNM for initial concentrations of *E. Coli* DH5 α of 0.05 optical density (OD) ($\sim 1.7 \times 10^8$ colony-forming units (CFU) mL $^{-1}$). The concentration of bacteria in the control group dramatically increases during the first 6 h, and then gradually stabilizes around 1.08 OD. The addition of Cu-Ag bimetallic PNMs below 100 mg L $^{-1}$ has little influence on the batch growth profile of *E. Coli* DH5 α . But the growth of the bacteria is significantly inhibited when the Cu-Ag bimetallic PNM's addition exceeds 200 mg L $^{-1}$. This result is consistent with the previous report that the concentration of Ag and Cu nanostructures has significant influence on their antibacterial activities.²⁹

Similar phenomenon was observed in the growth profile for initial concentrations of *E. Coli* DH5 α of 0.16 OD ($\sim 5.6 \times 10^8$ CFU mL $^{-1}$) (seeing Fig. 7b), indicating that the Cu-Ag bimetallic PNMs possess good antibacterial activity over a wide concentration range of bacteria. Compared with the growth profile for initial concentrations of *E. Coli* DH5 α of 0.05 OD, the surviving bacteria population is much larger under the addition of Cu-Ag bimetallic PNMs with a concentration of 200 mg L $^{-1}$, which also indicates that the concentration of the bacteria has significant influence on the antibacterial activities of the Cu-Ag bimetallic PNMs.

Discussions

Although the prepared Cu-Ag bimetallic PNMs exhibit mediocre antibacterial activity, the Cu-Ag bimetallic PNMs possess intact shape with a large-area of more than 20 square microns even after suffered from the ultrasonic vibration (as shown in the Fig. 2), indicating that the Cu-Ag bimetallic PNMs is quite stable. Thus, by designing the composition of MGs and selecting proper dealloying solutions and parameters, various large-area and stable multicomponent PNMs could be synthesized through the developed method of simple chemical dealloying assisted with ultrasonic vibration. The present work provided a new and simple method for the synthesis of multicomponent PNMs.

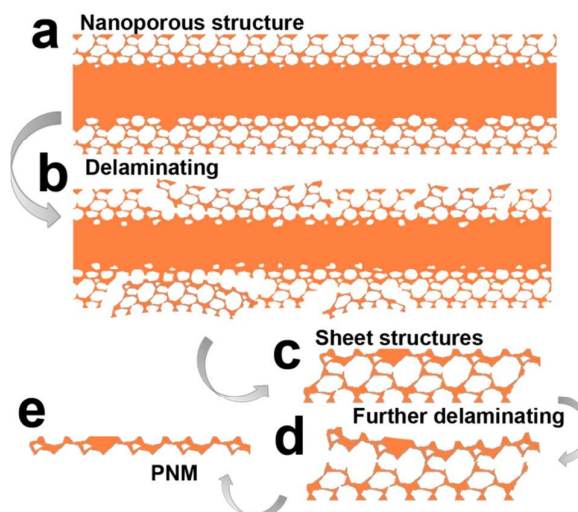


Fig. 6 Illustration of the evolution of the PNMs. (a) The formation of nanoporous structure. (b) The activation of delaminating. (c) The formation of sheet structure. (d) The activation of further delaminating. (e) The formation of PNM.

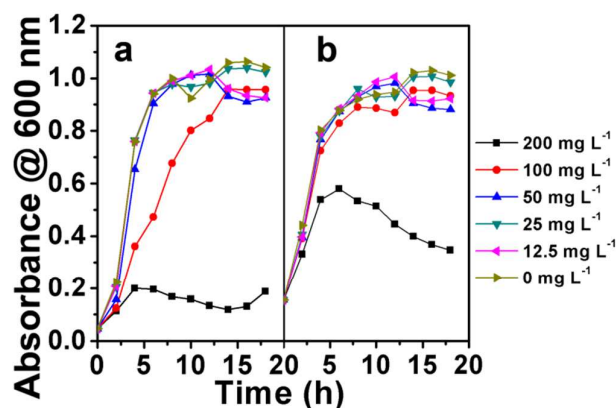


Fig. 7 Representative batch growth profiles in the presence of Cu-Ag bimetallic PNM for initial concentrations of *E. Coli* DH5 α : (a) 0.05 OD and (b) 0.16 OD.

Conclusions

Two dimensional ultrathin Cu-Ag bimetallic PNMs with an thickness of about 5~50 nm and an area larger than 20 square micron, together with pore diameter of ~ 10 -20 nm and ligament feature size of ~ 30 -50 nm, have been successfully prepared by chemical dealloying assisted with ultrasonic vibration from a $Zr_{48}Cu_{36}Ag_8Al_8$ metallic glassy ribbons. The effects of dealloying parameters on the dealloyed samples' morphology were systematically investigated. This work provides new and important insights into the easy and inexpensive synthesis of PNMs. The prepared Cu-Ag bimetallic PNMs exhibit good antibacterial activity against *E. coli* over a wide concentration range.

Experimental section

Preparing of $Zr_{48}Cu_{36}Ag_8Al_8$ MG ribbon

Alloys with a nominal composition of $Zr_{48}Cu_{36}Ag_8Al_8$ (at.%) were prepared by arc-melting the mixtures of pure Zr, Cu, Ag and Al (>99.4 mass%) in an argon atmosphere. To achieve chemical homogeneity, each ingot was remelted for at least 4 times. Then the $Zr_{48}Cu_{36}Ag_8Al_8$ ribbons with dimensions of ~8 mm in width and ~30 μ m in thickness were prepared by employing a single-roller melt-spinner.

Characterization of the $Zr_{48}Cu_{36}Ag_8Al_8$ MG ribbons

The structure of the prepared $Zr_{48}Cu_{36}Ag_8Al_8$ MG ribbons were examined by Rigaku D/max-RB XRD with Cu $K\alpha$ radiation at a scanning rate of 8 degrees per min and a detecting step of 0.02 degree.

Dealloying procedures

The $Zr_{48}Cu_{36}Ag_8Al_8$ MG ribbons were cut into ribbons with ~40 mm in length, and dealloyed in hydrofluoric acid solutions (0.01 M, 0.05 M and 0.2 M) for different time (1 h, 3 h, 6 h, 12 h and 24 h). After dealloying the ribbon samples were removed from the solution, washed in ethanol, and then dried in air. All experiments were performed at room temperature.

Characterization of the Cu-Ag bimetallic PNMs

The structures and the surfaces of the dealloyed samples were examined again by Rigaku D/max-RB XRD and LEO1530 SEM. Then the dealloyed samples were dispersed in ethanol by ultrasound vibration and then collected by a copper grid with holey carbon films for observation with a JEOL 2011 TEM.

Antibacterial activity testing of the Cu-Ag bimetallic PNMs

The antibacterial investigations on the Cu-Ag bimetallic PNMs were performed against *E. coli* DH5 α strains. Luria-Bertani (LB) medium was used as a carrier to dilute the Cu-Ag bimetallic PNMs solutions to different concentrations by ultrasonic vibration. The monoclonal *E. coli* DH5 α cells were grown over-night in 20 ml LB medium at 310 K on a Shaker (BHWY-100, Safe, Zhejiang, China), and then diluted to ODs of 0.15 and 0.05 (at the wavelength of 600 nm) with a volume of 20 ml by different Cu-Ag PNMs solution. Also the controls were prepared under the same conditions, *i.e.* bacteria, LB medium and water, but without supplements of Cu-Ag PNMs. Then the *E. coli* DH5 α cells were cultured at 310 K on the Shaker for 18 h. The change in the OD at the wavelength of 600 nm was monitored by using a UV-vis spectrophotometer (Unico 2800, Unico, Shanghai, China) with an interval of every 2 h.

Acknowledgements

This work was supported by the National Science Foundation of China (Grand No. 51271095, 51101090 and 31370018) and National Natural Science Foundation of Tsinghua University (2012Z02133).

Notes and references

- 1 M. Tchapyguine, T. Andersson, C. Zhang and O. Bjorneholm, *J. Chem. Phys.*, 2013, **138**, 104303.

- 2 S. Mukherjee, M. Carmo, G. Kumar, R. C. Sekol, A. D. Taylor and J. Schroers, *Electrochim. Acta*, 2012, **74**, 145-150.
- 3 X. Liu, Y. Shao, J. F. Li, N. Chen and K. F. Yao, *J. Alloys Compd.*, 2014, **605**, 7-11.
- 4 W. Wu, M. Lei, S. L. Yang, L. Zhou, L. Liu, X. H. Xiao, C. Z. Jiang and V. A. L. Roy, *J. Mater. Chem. A*, 2015, **3**, 3450-3455.
- 5 X. Liu, S. F. Zhao, Y. Shao and K. F. Yao, *RSC Adv.*, 2014, **4**, 33362-33365.
- 6 A. K. Geim and K. S. Novoselov, *Nat. Mater.*, 2007, **6**, 183-191.
- 7 V. Purushothaman, P. S. Venkatesh, R. Navamathavan and K. Jeganathan, *RSC Adv.*, 2014, **4**, 45100-45108.
- 8 S. N. Paglieri, N. K. Pal, M. D. Dolan, S. M. Kim, W. M. Chien, J. Lamb, D. Chandra, K. M. Hubbard and D. P. Moore, *J. Membr. Sci.*, 2011, **378**, 42-50.
- 9 Z. H. Liao, J. J. Chen, K. F. Yao, F. H. Zhao and R. X. Li, *J. Inorg. Mater.*, 2004, **19**, 749-754.
- 10 Z. H. Liao, J. J. Chen, K. F. Yao, F. H. Zhao and R. X. Li, *J. Inorg. Mater.*, 2004, **19**, 17-24.
- 11 X. M. Liu and K. F. Yao, *Nanotechnology*, 2005, **16**, 2932-2935.
- 12 X. L. Fan and K. F. Yao, *Chin. Sci. Bull.*, 2007, **52**, 2866-2870.
- 13 K. F. Yao, Z. Peng, Z. H. Liao and J. J. Chen, *J. Nanosci. Nanotechnol.*, 2009, **9**, 1458-1461.
- 14 M. H. Wang, F. Zhou and B. Zhang, *Mater. Lett.*, 2014, **114**, 84-87.
- 15 X. Liu, Y. Shao, P. Gong and K. F. Yao, *Mater. Lett.*, 2013, **93**, 103-106.
- 16 M. K. Song, P. Rai, K. J. Ko, S. H. Jeon, B. S. Chon, C. H. Lee and Y. T. Yu, *RSC Adv.*, 2014, **4**, 3529-3535.
- 17 J. Huang, F. Chen, Q. Zhang, Y. Zhan, D. Ma, K. Xu and Y. Zhao, *ACS Appl. Mater. Interfaces*, 2015, **7**, 5725-5735.
- 18 X. Liu, Y. Shao, Y. Tang and K. F. Yao, *Sci. Rep.*, 2014, **4**, 5835.
- 19 X. Liu, Y. Shao, Z. D. Han and K. F. Yao, *Sci. Bull.*, 2015, **60**, 629-633.
- 20 C. R. Martin, *Science*, 1994, **266**, 1961-1966.
- 21 C. R. Martin, *Chem. Mater.*, 1996, **8**, 1739-1746.
- 22 N. Hilal, H. Al-Zoubi, N. A. Darwish, A. W. Mohammad and M. Abu Arabi, *Desalination*, 2004, **170**, 281-308.
- 23 H. L. Cong, M. Radosz, B. F. Towler and Y. Q. Shen, *Sep. Purif. Technol.*, 2007, **55**, 281-291.
- 24 A. F. Ismail, P. S. Goh, S. M. Sanip and M. Aziz, *Sep. Purif. Technol.*, 2009, **70**, 12-26.
- 25 M. M. Pendergast and E. M. V. Hoek, *Energy Environ. Sci.*, 2011, **4**, 1946-1971.
- 26 E. Gulpepe, D. Nagesha, S. Sridhar and M. Amiji, *Adv. Drug Del. Rev.*, 2010, **62**, 305-315.
- 27 P. Kohli, M. Wirtz and C. R. Martin, *Electroanalysis*, 2004, **16**, 9-18.
- 28 W. L. Cheng, M. J. Campolongo, S. J. Tan and D. Luo, *Nano Today*, 2009, **4**, 482-493.
- 29 M. Taner, N. Sayar, I. G. Yulug and S. Suzer, *J. Mater. Chem.*, 2011, **21**, 13150-13154.

Journal Name

ARTICLE

- 30 S. Mallick, P. Sanpui, S. S. Ghosh, A. Chattopadhyay and A. Paul, *RSC Adv.*, 2015, **5**, 12268-12276.
- 31 I. Najdovski, P. R. Selvakannan and A. P. O'Mullane, *RSC Adv.*, 2014, **4**, 7207-7215.
- 32 S. Tanaka, T. Kaneko, N. Asao, Y. Yamamoto, M. W. Chen, W. Zhang and A. Inoue, *Chem. Commun.*, 2011, **47**, 5985-5987.
- 33 Q. S. Zhang, W. Zhang and A. Inoue, *Scripta Mater.*, 2006, **55**, 711-713.
- 34 H. Abe, K. Sato, H. Nishikawa, T. Takemoto, M. Fukuhara and A. Inoue, *Mater. Trans.*, 2009, **50**, 1255-1258.
- 35 J. Erlebacher, M. J. Aziz, A. Karma, N. Dimitrov and K. Sieradzki, *Nature*, 2001, **410**, 450-453.